

Dynamic Modeling and Parameter Estimation for Origami Structure Reconfiguration Process

Yuto Tanaka, Ran Dai, and Mehran Mesbahi

Abstract—The reconfiguration of origami during the folding and unfolding process is governed through a sequence of panel deformations and hinge orientations. To develop an effective model for representing the reconfiguration process, this paper introduces planar straight-line graphs and a novel consensus protocol for reaching the target origami configuration. The convergence and stability properties of the proposed consensus protocol are subsequently analyzed. Furthermore, to account for aggregate material and structural effects in the proposed consensus-based reconfiguration model, effective parameters embedded in the consensus protocol are identified from trajectory data using a fitting algorithm. Lastly, the effectiveness of the proposed modeling approach is shown using simulations of the two-panel structure and the Kresling origami pattern reconfiguration process.

I. INTRODUCTION

Origami, the traditional art of paper-folding, has recently become a multidisciplinary framework for designing novel mechanisms and engineering structures. Origami structural principles are used for example in robotics, biomedical devices, and aerospace engineering. From robotic systems [1] and foldable medical tools [2] to compact satellite components [3], origami-based designs stand out for their portability, adaptability, and efficiency [4], [5]. As the range of these applications expand, accurately modeling and predicting how origami structures behave under dynamic conditions has become essential.

Modeling approaches for origami systems generally fall into two categories: mechanics-based models, built on structural and material principles, and data-driven models that rely on observed system behavior. Mechanics-based frameworks, such as bar-and-hinge models, are particularly effective in capturing the kinematic constraints and physical motions associated with folding structures [6]–[8]. However, these models typically require detailed prior knowledge of material properties, such as Young’s modulus, to accurately represent the system’s behavior during the reconfiguration process. In addition, while bar-and-hinge models effectively characterize geometric and mechanical transformations, they often lack a comprehensive analysis of the system’s dynamic properties, indispensable for investigating their time-evolution.

Data-driven modeling approaches—including those based on the finite element method, machine learning and numerical

techniques—have shown strong predictive capabilities for complex systems [9]–[12]. However, these methods typically rely heavily on large volumes of high-quality data to capture the system dynamics accurately. As a result, the generalizability of the aforementioned methods is often limited to the range and conditions captured by the training data. Moreover, generating and preprocessing such data, particularly through high-fidelity simulations can be computationally expensive and time-consuming. By combining the motivation of exploring origami dynamic models with insights from data-driven methods, hybrid modeling approaches hold promise for creating more accurate and versatile representations of origami structures.

It is natural to represent origami structures using graph theory, where creases correspond to edges and crease intersections map to graph vertices. This connection has inspired a broad body of work at the intersection of origami and graph theory. On one hand, unit origami has served as an intuitive tool to teach fundamental graph theoretic concepts [13]; on the other hand, graph-theoretic methods have been employed to support origami design, providing mathematical insights into geometric and topological properties of foldable structures [14]–[18]. This paper presents a systematic approach to model the folding and unfolding processes of origami structures using dynamic networks and a new twist on the consensus protocol.

In an origami system, reconfiguration is achieved through panel deformations, namely expansion and contraction within individual two-dimensional (2D) planes and rotations along shared edges. However, the traditional consensus protocol adopted for three-dimensional (3D) space steers the coordinates of the vertices independently along each axis; specifically, the protocol does not restrict origami movement due to expansion/contraction within individual 2D panel surfaces [19]–[21]. Furthermore, the traditional consensus protocol cannot be applied directly to coordinate vertices for panel rotational movements around the hinges, as illustrated by comparative examples in the following context.

This work proposes a frame-projected consensus protocol (FPCP) to capture the complex and localized interactions between vertices during the origami reconfiguration process. This method projects each vertex into the frame of its corresponding panel, hence the name “frame projection” consensus. FPCP is employed in two distinct yet complementary forms: a triangulated consensus protocol for modeling panel deformations, and a hinge consensus protocol for capturing panel-to-panel rotational dynamics. The triangular consensus protocol defines the target configuration within each individual triangular panel surface, ensuring that vertex coordination, driven by panel deformation, occurs strictly within the local 2D frame of

Yuto Tanaka and Ran Dai are with the School of Aeronautics and Astronautics, Purdue University, West Lafayette, IN, 47907. Emails: tanaka9@purdue.edu, randai@purdue.edu

Mehran Mesbahi is with William E. Boeing Department of Aeronautics and Astronautics, University of Washington, Seattle, WA, 98195. Email: mesbahi@uw.edu

the panel. In parallel, the hinge consensus protocol specifies the desired equilibrium angle between adjacent panels and drives the shared vertices toward configurations that satisfy this target angular relationship, thereby capturing the panel rotational motion during the reconfiguration process. The proposed FPCP, which emphasizes geometric coordination within each panel surface and at inter-panel hinges, fundamentally differs from existing projection-based consensus protocols. Without accounting for the localized, structure-preserving requirements intrinsic to the origami reconfiguration, existing projection-based consensus protocols typically operate under global state constraints, such as projecting agents onto convex sets or maintaining predefined feasibility regions [21]–[24].

Multiple factors, for example, the properties of the origami structure, tessellation patterns, and panel sizes, affect the consensus speed of each vertex within the origami structure network [25]–[27]. To accurately capture the influence of all contributing factors, a data-fitting approach has been adopted to estimate the weighting factors embedded in the FPCP. Specifically, by measuring the coordinates of observed vertices in a time sequence, weights incorporated into the FPCP are estimated using the parameter optimization method to match the observation as closely as possible. The weighted FPCP (namely W-FPCP), as observed from existing weighted consensus protocols [28], [29], outperforms FPCP with uniform weights when representing the origami reconfiguration process, where vertices exhibit diverse dynamic behaviors.

Our prior work in [30] developed a dynamic model to represent the origami panel expansion/contraction process based on the triangulated consensus protocol. To model the entire system evolution, this work includes both panel deformation and hinge rotation using the unified FPCP approach. Furthermore, rigorous proof of the convergence of FPCP is provided. The contributions of this work are as follows: (1) design of FPCP that captures the panel deformation process occurring within their respective 2D surfaces, while also accounting for the rotation effects of the hinges; (2) proof of convergence of the proposed FPCP; and (3) development of a data-fitting approach to incorporate system parameters into the proposed FPCP.

Section II presents the preliminaries, including the properties of origami structures, the 3D-to-2D projection, and the network components associated with origami structures. Section III discusses the limitations of the traditional consensus protocol and introduces the proposed FPCP. Section IV incorporates weighting parameters into the FPCP, extends the protocol to the entire origami structure, and presents the convergence analysis and parameter estimation procedure. Section V provides simulation results, and Section VI concludes the paper.

II. PRELIMINARIES

In this section, we provide a concise overview of origami structures and their graph representation.

A. Origami Structure Properties

Origami-inspired structures exhibit two types of motion primitives that define their mechanical behavior during the

folding/unfolding process: panel deformation and panel rotation around hinges. These motions enable the structure to achieve complex folding and unfolding patterns while retaining certain levels of stability and adaptability.

The first type of movement, panel deformation, refers to the evolution of the panels to shrink or expand under external forces. This deformation is affected by material characteristics, geometric configuration, and boundary conditions of the panels. These factors dictate the flexibility and resilience of the structure, allowing it to adapt its shape in response to external stimuli while preserving its structural integrity.

The second type of motion, the rotation of the panels around the hinges, refers to the angular movement at the hinges that connect the panels; the angular motion is governed by the moments acting on the hinges. The equilibrium of these panel angles plays a critical role in determining how the structure transitions between folded and unfolded states. The interplay between the panel deformation and rotation defines the states of the overall origami structure during the reconfiguration process.

B. Graph Representation for Origami Structures

An origami configuration can be modeled as a planar straight-line graph, where edges represent the creases and vertices represent the points where these creases intersect. The complete set of all creases in an origami structure, typically visualized in a single diagram, is called the crease pattern and is denoted as \mathcal{C} . The crease pattern \mathcal{C} serves as a two-dimensional blueprint for the folding process, and it encodes the geometric information necessary for constructing the three-dimensional (3D) origami structure from a two-dimensional (2D) sheet.

Consider a multi-agent system, where $\mathbf{x}_i(t) \in \mathbb{R}^3$ denotes the coordinate of agent i at time t . In our setting, each agent i represents a vertex in a triangulated configuration consisting of three vertices. An origami structure can thus be regarded as a set of such triangulated configurations, denoted as $\mathcal{G} = (\mathcal{V}, \mathcal{E})$, where \mathcal{G} is a graph representing the connections between vertices corresponding to the creases of the origami, $\mathcal{V} = \{1, 2, \dots, n\}$ is the set of vertices representing the agents, and $\mathcal{E} \subseteq \mathcal{V} \times \mathcal{V}$ is the set of edges representing the incident relation between agents, e.g., $\{i, j\} \in \mathcal{E}$ for agents i and j . An example of the graph representation of Miura-ori pattern origami is shown in Fig. 1.

C. 3D to 2D Projection

Projection from 3D space to a 2D plane is used in this work when modeling the system dynamics; as such, in this section we introduce the coordinate conversion for mapping a point from 3D to 2D. The projection of points in a 3D space into a 2D plane is a fundamental operation in many geometric and computational problems.

To define the projection, we introduce two orthonormal vectors $\mathbf{w}_1, \mathbf{w}_2 \in \mathbb{R}^3$ that span the local 2D plane. These vectors form a basis for the plane onto which the 3D coordinates are projected. Together, these two normalized and mutually

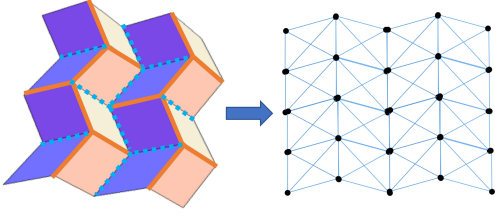


Fig. 1: An example of Miura-ori origami structure and its graph representation, where creases and crossbars represent edges, and nodes represent intersections of creases and crossbars; the “crossbars” decompose the quadrilateral into triangular sets and are used to (subsequently) capture the bending behavior of each panel.

orthogonal vectors form the basis of the 2D plane, as well as the projection conversion matrix $M \in \mathbb{R}^{2 \times 3}$, written as

$$M = [\mathbf{w}_1 \quad \mathbf{w}_2]^\top. \quad (1)$$

It thus follows that $MM^\top = I_2$, where $I_2 \in \mathbb{R}^{2 \times 2}$ is the 2×2 identity matrix. The projection conversion matrix constructed from these vectors serves as the foundation for mapping 3D points to the 2D plane, expressed as

$$\tilde{\mathbf{x}}_\iota = M\mathbf{x}_\iota, \quad (2)$$

where a 3D coordinate $\mathbf{x}_\iota \in \mathbb{R}^3$ is projected into a 2D plane with a coordinate $\tilde{\mathbf{x}}_\iota \in \mathbb{R}^2$.

III. FRAME PROJECTION CONSENSUS PROTOCOL

Consensus protocol is widely utilized in distributed multi-agent systems to achieve agreement among agents on a common state. Consider a network defined by a vertex set \mathcal{V} and edge set \mathcal{E} . The standard consensus protocol governing the dynamics of a system with n agents can be expressed as

$$\dot{\mathbf{x}}(t) = -L(\mathcal{G})\mathbf{x}(t), \quad (3)$$

where $\mathbf{x}(t) = [x_1(t), x_2(t), \dots, x_n(t)]^\top$ represents the states of the n agents, and $L(\mathcal{G})$ denotes the graph Laplacian associated with the network. Extending this concept to formation control, specifically for a triangular formation defined by the complete graph \mathcal{K}_3 , the consensus algorithm takes the form

$$\dot{\mathbf{x}}(t) = -L(\mathcal{K}_3)(\mathbf{x}(t) - \mathbf{r}), \quad (4)$$

where $\mathbf{r} = [r_{ij}]$, for $(i, j) \in \mathcal{E}$, specifies the desired relative positions between the agents. Under this protocol, the agents' states asymptotically converge to the target formation, achieving $\lim_{t \rightarrow \infty} (x_i(t) - x_j(t)) = r_{ij}$, for every edge $(i, j) \in \mathcal{E}$.

However, when employing the traditional consensus protocol for guiding vertices toward a geometric formation, vertex coordination occurs independently along each axis in the 3D space. Consequently, such coordination does not inherently restrict panel deformation to the intended 2D panel surfaces, failing to preserve the structural integrity during origami reconfiguration. Considering the limitations of traditional consensus protocols, we propose the FPCP that identifies the corresponding 2D projection planes where deformation or rotation of panels occurs. The consensus-based formation law is

then operated within the correct geometric surface to preserve structural integrity during the origami reconfiguration.

A. Triangulated Consensus Protocol

This section introduces the triangulated consensus protocol to model the panel deformation process. We start by assuming a connected triangular graph $\mathcal{G} = (\mathcal{V}, \mathcal{E})$ on three vertices ($n = 3$) with coordinates $\mathbf{x}_{i,j,k} = [\mathbf{x}_i^\top, \mathbf{x}_j^\top, \mathbf{x}_k^\top]^\top$, where $\mathbf{x}_\iota \in \mathbb{R}^3$, and $\iota = i, j, k$ designate the indices of these vertices. To project a 3D coordinate to a 2D triangular panel surface, we employ the projection conversion matrix defined in (1). In this case, the projection conversion matrix is determined by

$$M_{\text{panel}} = \begin{bmatrix} \frac{\mathbf{p}_{j,i}}{\|\mathbf{p}_{j,i}\|} & \frac{(\mathbf{p}_{j,i} \times \mathbf{p}_{k,i}) \times \mathbf{p}_{j,i}}{\|(\mathbf{p}_{j,i} \times \mathbf{p}_{k,i}) \times \mathbf{p}_{j,i}\|} \end{bmatrix}^\top, \quad (5)$$

where $M_{\text{panel}} \in \mathbb{R}^{2 \times 3}$, $\mathbf{p}_{\iota,\kappa} = \mathbf{x}_\iota - \mathbf{x}_\kappa$, $\iota, \kappa = i, j, k$, $\iota \neq \kappa$. Then the 2D coordinates of the vertices in individual triangular panel surfaces, denoted as $\tilde{\mathbf{x}}_{i,j,k} \in \mathbb{R}^2$, can be computed via

$$\tilde{\mathbf{x}}_{i,j,k} = \tilde{M}_{\text{panel}} \mathbf{x}_{i,j,k}, \quad (6)$$

where $\tilde{M}_{\text{panel}} = I_3 \otimes M_{\text{panel}}$, $I_3 \in \mathbb{R}^3$ is the 3×3 identity matrix, and ‘ \otimes ’ denotes the Kronecker product.

The traditional consensus protocol is now applied to the projected coordinates on the 2D plane, with respect to the desired planar triangular configuration, denoted by $\tilde{\mathbf{r}}_{i,j,k}^{\text{panel}\top} = [\tilde{\mathbf{r}}_i^{\text{panel}\top}, \tilde{\mathbf{r}}_j^{\text{panel}\top}, \tilde{\mathbf{r}}_k^{\text{panel}\top}]^\top$, with $\tilde{\mathbf{r}}_\iota^{\text{panel}} \in \mathbb{R}^2$, $\iota = i, j, k$. Furthermore, the relative vector $\tilde{\mathbf{r}}_j^{\text{panel}} - \tilde{\mathbf{r}}_i^{\text{panel}}$ is aligned with $\mathbf{p}_{i,j}$ such that

$$\tilde{\mathbf{r}}_j^{\text{panel}} - \tilde{\mathbf{r}}_i^{\text{panel}} = \alpha M_{\text{panel}} \mathbf{p}_{i,j}, \quad (7)$$

where $\alpha \in \mathbb{R}$ is a scalar. Lastly, we assume that $\tilde{\mathbf{r}}_i^{\text{panel}}$ overlaps with $M_{\text{panel}} \mathbf{x}_i$, i.e., $\tilde{\mathbf{r}}_i^{\text{panel}} = M_{\text{panel}} \mathbf{x}_i$. The alignment and overlap simply choose vertex i as the local reference point, so that the consensus law drives relative deformation rather than introducing an arbitrary in-plane shift.

Next, we apply the consensus protocol, in the context of formation control, to the projected coordinates of the origami panel. For a triangular (complete) graph \mathcal{K}_3 , the consensus interaction among the vertices is represented through the graph Laplacian $L(\mathcal{K}_3)$. The consensus dynamics on the projected 2D coordinates can therefore be written as

$$\dot{\tilde{\mathbf{x}}}_{i,j,k} = -L_2(\tilde{\mathbf{x}}_{i,j,k} - \tilde{\mathbf{r}}_{i,j,k}^{\text{panel}}), \quad (8)$$

where $L_2 = L(\mathcal{K}_3) \otimes I_2$. The velocity prescribed by the 2D consensus is then lifted back to the 3D space as,

$$\dot{\mathbf{x}}_{i,j,k} = \tilde{M}_{\text{panel}}^\top \dot{\tilde{\mathbf{x}}}_{i,j,k}. \quad (9)$$

In summary, the dynamics of the vertices based on the triangulated consensus assumes the form $\dot{\mathbf{x}}_{i,j,k} = f(\mathbf{x}_{i,j,k})$, where,

$$f_{\text{panel}}(\mathbf{x}_{i,j,k}) = -\tilde{M}_{\text{panel}}^\top L_2(\tilde{M}_{\text{panel}} \mathbf{x}_{i,j,k} - \tilde{\mathbf{r}}_{i,j,k}^{\text{panel}}). \quad (10)$$

Transformation from 3D to 2D coordinates using the projection matrix converts the origami panel representation from a global frame to its local frame. This approach enables capturing dynamic features that cannot be addressed using

the traditional consensus control, namely, driving to a target formation specified within a 2D plane.

To illustrate the working mechanism of the triangulated consensus protocol and its difference from traditional consensus, a comparative example is provided in Fig. 2. Consider a triangulated graph in Fig. 2(a), consisting of a target formation (blue) and the initial configuration of the graph (red panel on the left side at $t = 0$). According to the projection conversion matrix in (5), the orthogonal vectors \mathbf{w}_1 and \mathbf{w}_2 are defined in Fig. 2(b). Using the triangulated consensus protocol, nodes assume the target formation on the original panel surface without changing the panel orientation, as shown in Fig. 2(c). However, when applying the traditional consensus protocol in (4), the coordination process is accompanied by a 3D rotation before converging to the target shape shown in Fig. 2(d). Specifically, the unexpected 3D rotation using the traditional consensus protocol fails to capture this important aspect of the origami dynamics during panel expansion/contraction.

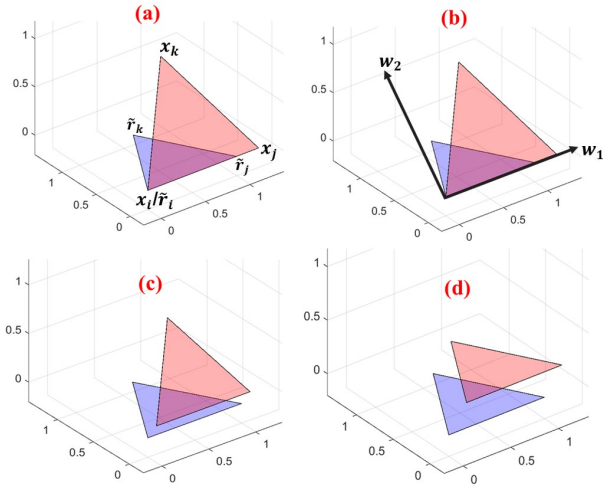


Fig. 2: An example to model origami panel deformation by applying triangulated consensus protocol (a)→(c), where consensus is applied to the local (x_i, x_j, x_k) plane; and traditional consensus protocol (a)→(d), where consensus is applied to the global 3D space.

B. Hinge Consensus Protocol

Hinge consensus aims to guide the structure in attaining the desired angles between two adjacent panels. The FPCP is then applied to two projected surfaces defined by four vertices, denoted i, j, k , and l . As shown in Fig. 3, the system configuration can be visualized as a diamond. The angle between two panels, composed of $\{l, k, j\}$ and $\{i, k, j\}$, is denoted by $\phi \in (-\pi, \pi]$. To drive the rotation of the two panels toward the equilibrium angle ϕ , two projection surfaces, composed of $\{i, k, l\}$ and $\{i, j, l\}$, are used to construct the two projection conversion matrices, denoted by M_{hinge1} and M_{hinge2} , respectively. These projection surfaces are chosen so that the hinge geometry is explicitly retained in the local construction: the hinge is the shared edge of the two adjacent panels, and the relevant motion is their relative rotation

about that common edge. Accordingly, the selected surfaces serve as auxiliary geometric frames anchored to the hinge configuration, allowing the planar target formations to encode the desired inter-panel angle rather than an arbitrary in-plane deformation. These matrices are defined as

$$M_{\text{hinge1}} = \begin{bmatrix} \frac{\mathbf{p}_{k,l}}{\|\mathbf{p}_{k,l}\|} & \frac{\mathbf{p}_{j,k} \times \mathbf{p}_{k,l}}{\|\mathbf{p}_{j,k} \times \mathbf{p}_{k,l}\|} \end{bmatrix}^\top, \quad (11a)$$

$$M_{\text{hinge2}} = \begin{bmatrix} \frac{\mathbf{p}_{j,i}}{\|\mathbf{p}_{j,i}\|} & \frac{\mathbf{p}_{i,j} \times \mathbf{p}_{k,j}}{\|\mathbf{p}_{i,j} \times \mathbf{p}_{k,j}\|} \end{bmatrix}^\top, \quad (11b)$$

where $\mathbf{p}_{\nu,\kappa} = \mathbf{x}_\nu - \mathbf{x}_\kappa$, $\nu, \kappa = i, j, k, l$, $\nu \neq \kappa$. The lifting in (11) should not be interpreted as a unique inverse from arbitrary 2D motions to arbitrary 3D motions. Rather, for any local frame used in the proposed protocol, let $M_\Gamma \in \{M_{\text{panel}}, M_{\text{hinge1}}, M_{\text{hinge2}}\}$. Once M_Γ is determined by the current local configuration, the projected consensus law prescribes an in-plane velocity in the corresponding local coordinates, and \tilde{M}_Γ^\top embeds this velocity back into the associated local subspace of \mathbb{R}^3 . Any component in $\ker(M_\Gamma)$, corresponding to the out-of-plane direction of the local frame, is therefore intentionally set to zero at this local update stage. Global compatibility across the origami structure is then enforced through the aggregation of local contributions at shared vertices in the full W-FPCP model discussed next.

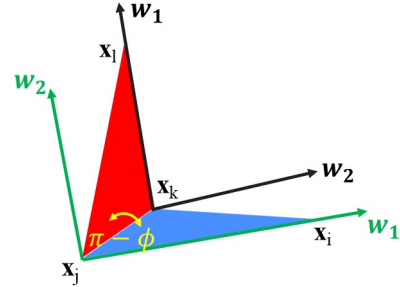


Fig. 3: Illustration of settings in the hinge consensus protocol.

After defining the two projection surfaces and their corresponding projection conversion matrices, the next step is to define the target formation, denoted by $\tilde{\mathbf{r}}_{i,k,l}$ and $\tilde{\mathbf{r}}_{i,j,l}$, respectively, creating a triangular shape with the target angle ϕ on each projection surface. To do so, we first use the equilibrium angle between the two panels to construct a rotation matrix from Rodrigues' rotation formula, expressed as

$$\begin{aligned} \Phi_\phi = I_3 \cos \phi + \left[\frac{\mathbf{q}_{k,j}}{\|\mathbf{q}_{k,j}\|} \right]_\times \sin \phi \\ + \left(\frac{\mathbf{q}_{k,j}}{\|\mathbf{q}_{k,j}\|} \right) \left(\frac{\mathbf{q}_{k,j}}{\|\mathbf{q}_{k,j}\|} \right)^\top (1 - \cos \phi), \end{aligned} \quad (12)$$

where $[\cdot]_\times$ denotes the skew-symmetric matrix and $\mathbf{q}_{\nu,\kappa} \in \mathbb{R}^3$ is a desired vector from vertex ν to κ at degree $\phi = 0$ for simplicity to represent the structure on a 2D plane to allow for $\phi \in (-\pi, \pi]$.

The positions of the target formation in the 2D projection planes are now defined as

$$\tilde{\mathbf{r}}_i^{\text{hinge1}} = \left\langle \left[\begin{array}{c} \frac{\mathbf{q}_{k,l}}{\|\mathbf{q}_{k,l}\|}, \Phi_\phi \mathbf{q}_{i,j} - \mathbf{q}_{k,j} \\ \frac{-\mathbf{q}_{k,j} \times \mathbf{q}_{k,l}}{\|-\mathbf{q}_{k,j} \times \mathbf{q}_{k,l}\|}, \Phi_\phi \mathbf{q}_{i,j} - \mathbf{q}_{k,j} \end{array} \right] \right\rangle^\top, \quad (13a)$$

$$\tilde{\mathbf{r}}_k^{\text{hinge1}} = [0 \ 0]^\top, \quad (13b)$$

$$\tilde{\mathbf{r}}_l^{\text{hinge1}} = [-\|\mathbf{q}_{k,l}\| \ 0]^\top, \quad (13c)$$

$$\tilde{\mathbf{r}}_i^{\text{hinge2}} = [-\|\mathbf{q}_{j,i}\| \ 0]^\top, \quad (13d)$$

$$\tilde{\mathbf{r}}_j^{\text{hinge2}} = [0 \ 0]^\top, \quad (13e)$$

$$\tilde{\mathbf{r}}_l^{\text{hinge2}} = \left[-\left\langle \frac{\Phi_\phi \mathbf{q}_{i,j}}{\|\Phi_\phi \mathbf{q}_{i,j}\|}, \mathbf{q}_{l,j} \right\rangle \ \left\langle \frac{\Phi_\phi \mathbf{q}_{i,j} \times \mathbf{q}_{k,j}}{\|\Phi_\phi \mathbf{q}_{i,j} \times \mathbf{q}_{k,j}\|}, \mathbf{q}_{l,j} \right\rangle \right]^\top. \quad (13f)$$

where $\langle \cdot, \cdot \rangle$ denotes the inner product between two vectors. Each vector defines the position of an element in the target formation, expressed in the local 2D plane corresponding to the side view of the two panels for the given angle ϕ .

Then, the target triangular formation is determined by

$$\tilde{\mathbf{r}}_{i,k,l}^{\text{hinge1}} = \begin{bmatrix} \tilde{\mathbf{r}}_i^{\text{hinge1}\top} & \tilde{\mathbf{r}}_k^{\text{hinge1}\top} & \tilde{\mathbf{r}}_l^{\text{hinge1}\top} \end{bmatrix}^\top, \quad (14a)$$

$$\tilde{\mathbf{r}}_{i,j,l}^{\text{hinge2}} = \begin{bmatrix} \tilde{\mathbf{r}}_i^{\text{hinge2}\top} & \tilde{\mathbf{r}}_j^{\text{hinge2}\top} & \tilde{\mathbf{r}}_l^{\text{hinge2}\top} \end{bmatrix}^\top. \quad (14b)$$

The definition of the target formation $\tilde{\mathbf{r}}_{i,k,l}^{\text{hinge1}}$ ensures that the angle between vectors $\tilde{\mathbf{r}}_i^{\text{hinge1}} - \tilde{\mathbf{r}}_k^{\text{hinge1}}$ and $\tilde{\mathbf{r}}_l^{\text{hinge1}} - \tilde{\mathbf{r}}_k^{\text{hinge1}}$ is the desired angle ϕ . Meanwhile, the definition of target formation $\tilde{\mathbf{r}}_{i,j,l}^{\text{hinge2}}$ ensures that the angle between vectors $\tilde{\mathbf{r}}_i^{\text{hinge2}} - \tilde{\mathbf{r}}_j^{\text{hinge2}}$ and $\tilde{\mathbf{r}}_l^{\text{hinge2}} - \tilde{\mathbf{r}}_j^{\text{hinge2}}$ is the desired angle ϕ as well.

Next, we apply the same consensus protocol in each projection plane, written as

$$f_{\text{hinge1}}(\mathbf{x}_{i,k,l}) = -\tilde{M}_{\text{hinge1}}^\top L_2(\tilde{M}_{\text{hinge1}} \mathbf{x}_{i,k,l} - \tilde{\mathbf{r}}_{i,k,l}^{\text{hinge1}}), \quad (15a)$$

$$f_{\text{hinge2}}(\mathbf{x}_{i,j,l}) = -\tilde{M}_{\text{hinge2}}^\top L_2(\tilde{M}_{\text{hinge2}} \mathbf{x}_{i,j,l} - \tilde{\mathbf{r}}_{i,j,l}^{\text{hinge2}}). \quad (15b)$$

The formation coordination in both projection planes will drive the two panels $\{l, k, j\}$ and $\{i, k, j\}$ toward the target angle ϕ . One example is shown in Fig. 4, where the hinge, initially positioned at 90 degrees, attempts to converge to its equilibrium angle of 180 degrees as $t \rightarrow \infty$.

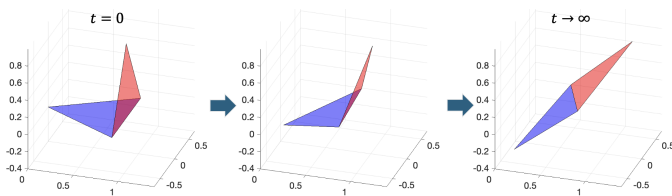


Fig. 4: An example of applying the hinge consensus protocol to origami panel rotations.

IV. WEIGHTED FRAME PROJECTED CONSENSUS FOR ORIGAMI DYNAMICS

The triangulated consensus and hinge consensus protocols introduced above are applicable to a single panel deformation

and panel rotations around one hinge, respectively. In meantime, factors that influence the speed of each vertex during the reconfiguration have not been considered in these protocols. The weighted frame projection consensus protocol (W-FPCP) is a framework designed to apply the FPCP to the entire origami system while incorporating parameters that capture each panel's deformation properties and enhance the modeling fidelity of the protocol. In particular, the weighted consensus protocol assigns effective interaction coefficients to the edges of the triangular graph to improve trajectory reproduction while accounting, in an aggregate phenomenological sense, for effects associated with strain-energy-related behavior, stiffness variation, hinge resistance, and material heterogeneity. These weights are not introduced as direct one-to-one physical stiffness or damping parameters with prescribed mechanical units derived from a first-principles model; instead, they are treated as fitted effective parameters within the proposed consensus-based reconfiguration model. By embedding these parameters into the reconfiguration process, the model not only achieves higher accuracy and adaptability, but also allows for the representation of diverse origami configurations. The weighted Laplacian, denoted $\Omega(\mathcal{K}_3) \in \mathbb{R}^{3 \times 3}$, for the triangular graph is used to replace the unweighted Laplacian $L(\mathcal{K}_3)$, expressed as

$$\Omega(\mathcal{K}_3) = \begin{bmatrix} \omega_{i,j} + \omega_{i,k} & -\omega_{i,j} & -\omega_{i,k} \\ -\omega_{i,j} & \omega_{i,j} + \omega_{j,k} & -\omega_{j,k} \\ -\omega_{i,k} & -\omega_{j,k} & \omega_{i,k} + \omega_{j,k} \end{bmatrix}, \quad (16)$$

where $\omega_{\ell,\kappa} = \omega_{\kappa,\ell} \geq 0$, $\ell, \kappa = i, j, k$, $\ell \neq \kappa$, are weights of the undirected graph corresponding to vertices ℓ and κ . To extend the weighted Laplacian to a triangular graph on a 2D plane, analogous to L_2 in (10), we define $\Omega_{i,j,k} \in \mathbb{R}^{6 \times 6}$, written as

$$\Omega_{i,j,k} = \begin{bmatrix} \omega_{i,j} + \omega_{i,k} & 0 & -\omega_{i,j} \\ 0 & \gamma_{i,j} + \gamma_{i,k} & 0 \\ -\omega_{i,j} & 0 & \omega_{i,j} + \omega_{j,k} \\ 0 & -\gamma_{i,j} & 0 \\ -\omega_{i,k} & 0 & -\omega_{j,k} \\ 0 & -\gamma_{i,k} & 0 \\ 0 & -\omega_{i,k} & 0 \\ -\gamma_{i,j} & 0 & -\gamma_{i,k} \\ 0 & -\omega_{j,k} & 0 \\ \gamma_{i,j} + \gamma_{j,k} & 0 & -\gamma_{j,k} \\ 0 & \omega_{i,k} + \omega_{j,k} & 0 \\ -\gamma_{j,k} & 0 & \gamma_{i,k} + \gamma_{j,k} \end{bmatrix}, \quad (17)$$

where elements $\omega_{\ell,\kappa} \geq 0$ and $\gamma_{\ell,\kappa} \geq 0$, $\ell, \kappa = i, j, k$, $\ell \neq \kappa$, denote weights along the two coordinates on a 2D plane, respectively. Since the graph is undirected, we assume $\omega_{\ell,\kappa} = \omega_{\kappa,\ell}$ and $\gamma_{\ell,\kappa} = \gamma_{\kappa,\ell}$ so that $\Omega_{i,j,k}$ is symmetric and positive semidefinite. The approach to determining these weights is addressed in §V to capture variations of panel properties. With the introduced weighted Laplacian representing weights for a triangular graph on a 2D plane, the frame projected consensus is then updated via

$$\dot{\mathbf{x}}_{i,j,k} = -\tilde{M}_{i,j,k}^\top \Omega_{i,j,k} \tilde{M}_{i,j,k} (\mathbf{x}_{i,j,k} - \tilde{M}_{i,j,k}^\top \tilde{\mathbf{r}}_{i,j,k}), \quad (18)$$

where $\tilde{M}_{i,j,k} = I_3 \otimes M_{i,j,k} \in \mathbb{R}^{6 \times 9}$ and $M_{i,j,k} \in \mathbb{R}^{2 \times 3}$ is the projection conversion matrix for the 2D panel composed by vertices $\{i, j, k\}$.

A. W-FPCP for Entire Origami Structure

The W-FPCP is applied individually to each panel deformation or rotation around the hinge above, ensuring that the dynamics of local interactions are accurately captured. By accounting for the cumulative contributions of each panel's deformation and rotation about every hinge, we synthesize the collective dynamics of the entire origami structure. The resulting comprehensive model accounts for the interplay between panels and hinges, as well as their shared constraints. Let the index of m panels and h hinges be denoted by $\Gamma = 1, \dots, m + 2h$ as each hinge consensus protocol requires consensus coordination twice as discussed in Section III-B; the overall system dynamics is now written as

$$\dot{\mathbf{x}} = \sum_{\Gamma=1}^{m+2h} (S_{i,j,k} \otimes I_3) \dot{\mathbf{x}}_{i,j,k}^{(\Gamma)}, \quad (19)$$

where $\mathbf{x} \in \mathbb{R}^{3\nu}$ is the stacked state vector for ν vertices within the entire origami structure, $S_{i,j,k} \in \mathbb{R}^{\nu \times 3}$ is a selection matrix with all entries set to zero except $S_{i,j,k}(i, 1) = S_{i,j,k}(j, 2) = S_{i,j,k}(k, 3) = 1$. The selection matrix is required to align the local vertices $\mathbf{x}_{i,j,k}^{(\Gamma)}$ in every triangular graph with the corresponding vertices in the stacked state vector \mathbf{x} . For each formation (panel or hinge) $\Gamma = 1, \dots, m + 2h$, the corresponding graph is $\mathcal{G}^{(\Gamma)} = (\mathcal{V}^{(\Gamma)}, \mathcal{E}^{(\Gamma)})$, where $\mathcal{V}^{(\Gamma)} = \{i, j, k\}$ denotes the three vertices of the triangular graph and $\mathcal{E}^{(\Gamma)}$ represents the edges that connect them. The term $\dot{\mathbf{x}}_{i,j,k}^{(\Gamma)}$ follows the W-FPCP in (18) for panel Γ . Using (19), the dynamics of the entire origami structure can be determined by accumulating the contributions of each local set of triangular vertices. Because adjacent panels share common vertices in the aggregated formulation, the motion of each such vertex is influenced by all incident local contributions, which enforces kinematic consistency at the shared-vertex level throughout the evolution. As a result, the global structure connectivity is guaranteed by the the shared-vertex aggregation formulation.

The traditional consensus protocol in (3) operates as a linear system governed by a more streamlined relationship between the states and their evolution. However, after incorporating the projection conversion matrix, the dynamics becomes nonlinear, introducing new types of dynamic phenomena. To obtain a compact form of the corresponding system dynamics, a series of conversions is introduced below to transform the system dynamics into a state-space representation.

For every $\dot{\mathbf{x}}_{i,j,k}^{(\Gamma)}$, $\Gamma = 1, \dots, m + 2h$, expressed in (19), we rewrite it as

$$\dot{\mathbf{x}}_{i,j,k}^{(\Gamma)} = -W_{i,j,k} \mathbf{x}_{i,j,k}^{(\Gamma)} - W_{i,j,k} \mathbf{b}_{i,j,k}, \quad (20)$$

where $W_{i,j,k} = \tilde{M}_{i,j,k}^\top \Omega_{i,j,k} \tilde{M}_{i,j,k} \in \mathbb{R}^{9 \times 9}$, $\mathbf{b}_{i,j,k} = -\tilde{M}_{i,j,k}^\top \tilde{\mathbf{r}}_{i,j,k}^{(\Gamma)} \in \mathbb{R}^9$ for all $\mathcal{V}^{(\Gamma)} = \{i, j, k\}$. To account for the accumulative effect from every $\dot{\mathbf{x}}_{i,j,k}^{(\Gamma)}$, $\Gamma = 1, \dots, m + 2h$,

to the stacked state \mathbf{x} , $W_{i,j,k}$ is expanded to $\hat{W}_{i,j,k} \in \mathbb{R}^{3\nu \times 3\nu}$ by first decomposing $W_{i,j,k}$ into

$$W_{i,j,k} = \sum_{\iota=1}^3 \sum_{\kappa=1}^3 G_{\iota,\kappa} \otimes W_{\iota,\kappa}, \quad (21)$$

where selection $G_{\iota,\kappa} \in \mathbb{R}^{3 \times 3}$ with all entries set to zero except $G_{\iota,\kappa}(\iota, \kappa) = 1$ and $W_{\iota,\kappa} \in \mathbb{R}^{3 \times 3}$ is the affect of consensus on agent ι on κ . From this, we expand the stacked state \mathbf{x} . The local interaction matrix $W_{i,j,k}$ can be embedded into the global system dynamics using a Kronecker-product representation. Thus, $W_{i,j,k}$ is expanded to $\hat{W}_{i,j,k} \in \mathbb{R}^{3\nu \times 3\nu}$, written as

$$\hat{W}_{i,j,k} = \sum_{\iota \in \mathcal{V}^{(\Gamma)}} \sum_{\kappa \in \mathcal{V}^{(\Gamma)}} \hat{G}_{\iota,\kappa} \otimes W_{\iota,\kappa}, \quad (22)$$

where $\hat{G}_{\iota,\kappa} \in \mathbb{R}^{\nu \times \nu}$ is a selection matrix with all entries set to zero except $\hat{G}_{\iota,\kappa}(\iota, \kappa) = 1$. Then $\mathbf{b}_{i,j,k}$ is expanded to $\hat{\mathbf{b}}_{i,j,k} \in \mathbb{R}^{3\nu}$, written as

$$\hat{\mathbf{b}}_{i,j,k} = (S_{i,j,k}^{(\Gamma)} \otimes I_3) \mathbf{b}_{i,j,k}. \quad (23)$$

Through the expansion of matrices, the system dynamics in (19) is written as

$$\dot{\mathbf{x}} = \sum_{\Gamma=1}^{m+2h} -\hat{W}_{i,j,k} (\mathbf{x} + \hat{\mathbf{b}}_{i,j,k}). \quad (24)$$

Next, by augmenting the system state vector to incorporate a constant term, denoted by $\hat{\mathbf{x}} = \begin{bmatrix} \mathbf{x} \\ 1 \end{bmatrix} \in \mathbb{R}^{3\nu+1}$, the system dynamics in (24) can be converted into a homogeneous form,

$$\dot{\hat{\mathbf{x}}} = A \hat{\mathbf{x}}, \quad (25)$$

where

$$A = \sum_{\Gamma=1}^{m+2h} A_{i,j,k}^{(\Gamma)} \in \mathbb{R}^{(3\nu+1) \times (3\nu+1)}$$

and

$$A_{i,j,k}^{(\Gamma)} = \begin{bmatrix} -\hat{W}_{i,j,k} & -\hat{W}_{i,j,k} \hat{\mathbf{b}}_{i,j,k} \\ \mathbf{0}_{1 \times 3\nu} & \mathbf{0}_{1 \times 1} \end{bmatrix},$$

with $\mathcal{V}^{(\Gamma)} = \{i, j, k\}$. The time-varying linear representation of W-FPCP derived above now facilitates its convergence analysis described next.

B. Convergence of W-FPCP

This section examines the convergence property of the origami dynamic model based on W-FPCP. In particular, we start with the convergence proof of triangulated consensus in (10) applied to a single panel and then extend to W-FPCP in (18) for one single panel. After that, we establish the convergence for the aggregated W-FPCP applied to the overall system under mild conditions.

Lemma IV.1. *The matrices $W_{i,j,k} = \tilde{M}_{i,j,k}^\top \Omega_{i,j,k} \tilde{M}_{i,j,k} \in \mathbb{R}^{9 \times 9}$ and $\Omega_{i,j,k} \in \mathbb{R}^{6 \times 6}$ defined in (17) and (18), respectively, share the same nonzero eigenvalues. In addition, $W_{i,j,k}$ is positive semidefinite since $\Omega_{i,j,k}$ is positive semidefinite.*

Proof. This follows from a classical property of matrix similarity in reduced dimensions: for matrices $C \in \mathbb{R}^{n \times m}$ and

$D \in \mathbb{R}^{m \times n}$, the nonzero eigenvalues of $CD \in \mathbb{R}^{n \times n}$ and $DC \in \mathbb{R}^{m \times m}$ are identical (including multiplicities). Applying this to our case, we obtain

$$\lambda_{\text{nz}}(\tilde{M}_{i,j,k}^\top \Omega_{i,j,k} \tilde{M}_{i,j,k}) = \lambda_{\text{nz}}(\tilde{M}_{i,j,k} \tilde{M}_{i,j,k}^\top \Omega_{i,j,k}), \quad (26)$$

where $\lambda_{\text{nz}}(\cdot)$ denotes the set of nonzero eigenvalues. Since $\tilde{M}\tilde{M}^\top = I_6$ (using the definitions of M and \tilde{M}), it follows that

$$\lambda_{\text{nz}}(\tilde{M}_{i,j,k}^\top \Omega_{i,j,k} \tilde{M}_{i,j,k}) = \lambda_{\text{nz}}(\Omega_{i,j,k}). \quad (27)$$

Thus, $\tilde{M}_{i,j,k}^\top \Omega_{i,j,k} \tilde{M}_{i,j,k}$ and $\Omega_{i,j,k}$ share the same set of nonzero eigenvalues. In addition, as $\tilde{M}_{i,j,k}^\top \Omega_{i,j,k} \tilde{M}_{i,j,k} = (\tilde{M}_{i,j,k}^\top \Omega_{i,j,k} \tilde{M}_{i,j,k})^\top$, $W_{i,j,k}$ is symmetric with non-negative eigenvalues. Thus, $W_{i,j,k}$ is positive semidefinite. \square

Corollary IV.1.1. *The matrices $\Omega_{i,j,k} \in \mathbb{R}^{6 \times 6}$ and $\hat{W}_{i,j,k} \in \mathbb{R}^{3\nu \times 3\nu}$ share the same set of nonzero eigenvalues. In addition, $\hat{W}_{i,j,k}$ is positive semidefinite.*

Proof. The embedding from $W_{i,j,k}$ to $\hat{W}_{i,j,k}$ as defined in (17) and (22) only places the local interaction matrix into the rows and columns corresponding to the coordinates of vertices i, j, k . Permutation similarity preserves the characteristic polynomial and hence the eigenvalues [31, Sec. 1.3]. Therefore, $\det(\lambda I_{3\nu} - \hat{W}_{i,j,k}) = \lambda^{3\nu-9} \det(\lambda I_9 - W_{i,j,k})$. we have $\lambda_{\text{nz}}(\hat{W}_{i,j,k}) = \lambda_{\text{nz}}(W_{i,j,k})$. From Lemma IV.1, we have $\lambda_{\text{nz}}(\tilde{M}_{i,j,k}^\top \Omega_{i,j,k} \tilde{M}_{i,j,k}) = \lambda_{\text{nz}}(\Omega_{i,j,k})$. As $W_{i,j,k} = \tilde{M}_{i,j,k}^\top \Omega_{i,j,k} \tilde{M}_{i,j,k}$, it thus follows that $\lambda_{\text{nz}}(\Omega_{i,j,k}) = \lambda_{\text{nz}}(\hat{W}_{i,j,k})$. As $\hat{W}_{i,j,k}$ is symmetric with non-negative eigenvalues, $\hat{W}_{i,j,k}$ is positive semidefinite. \square

Next, we first examine the convergence of FPCP applied to a single panel, i.e., the consensus protocols in (10) and (15). Without loss of generality, we focus on the convergence of triangulated consensus in (10).

Theorem IV.2 (Theorem 5.1 in [30]). *Consider the triangulated consensus dynamics in (10), where M_{panel} and $\tilde{\mathbf{r}}_{i,j,k}^{\text{panel}}$ are fixed during the local panel update. Then the projected relative coordinates converge to the desired triangular formation, i.e.,*

$$M_{\text{panel}}(\mathbf{x}_\iota(t) - \mathbf{x}_\kappa(t)) \rightarrow \tilde{\mathbf{r}}_\iota^{\text{panel}} - \tilde{\mathbf{r}}_\kappa^{\text{panel}}, \quad \iota, \kappa \in \{i, j, k\}.$$

Equivalently, the projected configuration converges to the desired formation up to a translation in the local 2D frame.

The proof of Theorem IV.2 is deferred to Appendix I.

Next, we will extend the convergence analysis to the weight-FPCP applied to a single panel.

Corollary IV.2.1 (Convergence of the local W-FPCP). *Consider the local W-FPCP dynamics in (18), where $\Omega_{i,j,k}$ in (17) is symmetric positive semidefinite and satisfies*

$$\ker(\Omega_{i,j,k}) = \{(\mathbf{1}_3 \otimes I_2)\mathbf{c} : \mathbf{c} \in \mathbb{R}^2\}. \quad (28)$$

Then the projected relative coordinates converge to the desired weighted formation, namely,

$$M_{i,j,k}(\mathbf{x}_\iota(t) - \mathbf{x}_\kappa(t)) \rightarrow \tilde{\mathbf{r}}_\iota - \tilde{\mathbf{r}}_\kappa, \quad \iota, \kappa \in \{i, j, k\}.$$

Equivalently, the local W-FPCP converges to the desired projected formation up to a rigid translation in the local 2D frame.

The proof of Corollary IV.2.1 is deferred to Appendix II.

Lastly, we examine the convergence of the aggregated W-FPCP in (25) for the entire system, considering all panels and hinges.

Assumption IV.3. *Consider the aggregated W-FPCP dynamics in (25) over a sequence of time intervals $[t_q, t_{q+1})$, $q = 0, 1, \dots$, with $t_q \rightarrow \infty$. The target formation $\tilde{\mathbf{r}}_{i,j,k}^{(\Gamma)}$, $\Gamma = 1, \dots, m + 2h$, is fixed for the entire time. On each interval, the states are updated with fixed projection matrices. According to (24), the dynamics for each time interval is rewritten as*

$$\dot{\mathbf{x}} = - \sum_{\Gamma=1}^{m+2h} \hat{W}_{\Gamma,q}(\mathbf{x} + \mathbf{b}_{\Gamma,q}), \quad t \in [t_q, t_{q+1}), \quad (29)$$

with subsystem $\mathcal{V}^{(\Gamma)} = \{i, j, k\}$, $\Gamma = 1, \dots, m + 2h$.

Assumption IV.3 implies that for each time interval q , the system dynamics (29) during that interval is a linear dynamical system, as the projection matrices hold constant. Thus, over the entire time, this assumption implies that the system has piecewise-linear dynamics. Given that the target formation $\tilde{\mathbf{r}}_{i,j,k}^{(\Gamma)}$, $\Gamma = 1, \dots, m + 2h$, is fixed for the entire time, we have the following common-equilibrium assumption.

Assumption IV.4. *For the dynamical system in (29), there exists a compatible equilibrium \mathbf{x}^* such that*

$$H_q \mathbf{x}^* = \mathbf{g}_q, \quad \forall q \geq 0, \quad (30)$$

where $H_q := \sum_{\Gamma=1}^{m+2h} \hat{W}_{\Gamma,q}$, and $\mathbf{g}_q := - \sum_{\Gamma=1}^{m+2h} \hat{W}_{\Gamma,q} \mathbf{b}_{\Gamma,q}$.

Theorem IV.5 (Convergence of the aggregated W-FPCP). *Under Assumptions IV.3 and IV.4, let \mathcal{N} denote the fixed null-motion subspace associated with global motion of the aggregated origami model. We assume that the fixed aggregated matrices H_q at each time interval $[t_q, t_{q+1})$ have a common nullspace,*

$$\ker(H_q) = \mathcal{N}, \quad \forall q \geq 0.$$

Assume that there exists $\mu > 0$ such that

$$\mathbf{e}^\top H_q \mathbf{e} \geq \mu \|\mathbf{e}\|^2, \quad \forall \mathbf{e} \in \mathcal{N}^\perp, \quad \forall q \geq 0. \quad (31)$$

Then the component of $\mathbf{x}(t) - \mathbf{x}^$ orthogonal to \mathcal{N} converges to zero, i.e., $P_{\mathcal{N}^\perp}(\mathbf{x}(t) - \mathbf{x}^*) \rightarrow 0$. Hence $\mathbf{x}(t)$ converges to the affine equilibrium set $\mathbf{x}^* + \mathcal{N}$.*

The proof of Theorem IV.5 is deferred to Appendix III.

C. Parameter Determination for Weights of FPCP

The edge weights embedded in each 6×6 weighted Laplacian $\Omega_{i,j,k}$ governs how fast and in which directions the vertices move under the FPCP protocol. Determining these weights is therefore important for improving the trajectory-reproduction fidelity of the proposed consensus-based re-configuration model. Consistent with the effective-parameter interpretation above, these weights are identified from trajectory data. With captured vertex trajectories, the weight determination problem can be formulated as an optimization

problem. Specifically, the weights are chosen to minimize differences between the predictions of the consensus model and the observed vertex trajectories. This subsection provides the mathematical formulation of the corresponding parameter-estimation problem and examines how parameter optimization can improve the fidelity of the proposed consensus-based reconfiguration model.

Assume that the coordinates of all vertices are observed at discrete times t_κ , $\kappa = 1, \dots, K$, with intervals $\Delta t_\kappa = t_{\kappa+1} - t_\kappa$. Denote the experimentally measured vertex coordinates at each time step as $\mathbf{y}(t_\kappa) \in \mathbb{R}^{3\nu+1}$. Correspondingly, the theoretical prediction from the consensus-based discrete-time model is denoted as $\mathbf{x}(t_\kappa) \in \mathbb{R}^{3\nu+1}$, whose evolution is governed by discretizing the continuous system dynamics in (25), expressed as

$$\mathbf{x}(t_{\kappa+1}) = (I_{3\nu+1} + A(\Omega)\Delta t_\kappa) \mathbf{x}(t_\kappa)$$

where $A(\Omega) = \sum_{\Gamma=1}^{m+2h} A_{i,j,k}^{(\Gamma)}(\Omega)$, and each component matrix $A_{i,j,k}^{(\Gamma)}(\omega)$ depends on the corresponding project conversion matrix and weight parameters $\Omega^{(\Gamma)}$, $\Gamma = 1, \dots, m + 2h$.

The parameter optimization aims to find the optimal set of weights $\Omega^{(\Gamma)}$ that minimize the cumulative mismatch between observed and predicted vertex positions. In summary, the parameter optimization problem is formulated as

$$\min_{\Omega^{(1)}, \dots, \Omega^{(m+2h)}} \sum_{\kappa=1}^K \|\mathbf{y}(t_\kappa) - \mathbf{x}(t_\kappa)\|_2 \quad (32a)$$

$$\text{s.t. } \mathbf{x}(t_{\kappa+1}) = (I_{3\nu+1} + A\Delta t_\kappa) \mathbf{x}(t_\kappa) \\ \kappa = 1, \dots, K. \quad (32b)$$

This constrained optimization problem can be formulated as nonlinear program (NLP) due to the bilinear dependence of the system states and the weights within the optimization. Existing NLP solvers, e.g., SNOPT, can efficiently address such problems and are employed to solve the optimization numerically.

V. SIMULATION RESULTS

To demonstrate the effectiveness of W-FPCP in representing origami reconfiguration dynamics, we consider two representative cases: a simplified two-panel structure and a Kresling pattern. The two-panel structure is used as a physics-based benchmark, where the reference trajectory is generated from a bar-and-hinge mechanics model. This benchmark directly evaluates whether W-FPCP can reproduce vertex-coordinate trajectories generated by mechanical effects such as hinge stiffness, damping, and inertia. The Kresling pattern is then used to evaluate the proposed framework on a more complex origami reconfiguration process. Since a calibrated physics-based bar-and-hinge with known material, hinge, damping, and inertia parameters is not available for the Kresling structure considered here, we use time-discretized geometric reconfiguration data for parameter identification and trajectory comparison. Therefore, the Kresling example should be interpreted as a calibrated trajectory-reproduction study, while the two-panel case provides the mechanics-based validation benchmark. Since the W-FPCP model in (25) is an autonomous dynamical system

without external control input, both simulation cases present the folding/unfolding process from an intermediate unstable state to a stable equilibrium state without external control.

A. Two-Panel Structure

We first evaluate the proposed W-FPCP on a simplified two-panel origami structure with a mechanics-based reference trajectory. The structure consists of two triangular panels connected by a shared hinge. This example captures the essential hinge-driven unfolding behavior while allowing the reference trajectory to be generated from a bar-and-hinge model that includes mechanical effects such as hinge stiffness, damping, and inertia derived from [6].

In the bar-and-hinge model, the two panels rotate about the shared hinge from an initial fold angle of 100° toward the equilibrium angle 180° , as shown Fig. 7. The mechanical parameters used in the bar-and-hinge simulation, including the panel geometry, bar stiffness, hinge stiffness, damping coefficient, and time step, are summarized in Table I. The resulting time histories of the panel vertices are used as the mechanics-based reference trajectory.

Parameter	Number	Unit
Axial bar stiffness	1.0×10^4	N/m
Rotational hinge stiffness	10	N m/rad
Time step	0.01	s
Translational damping coefficient	6.0	N s/m

TABLE I: Physical parameters used in the bar-and-hinge dynamic model.

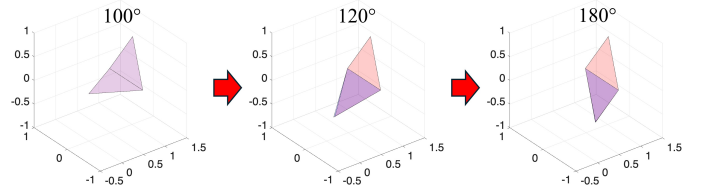


Fig. 5: Reference bar-and-hinge model (red) and calculated (blue) states of the two-panel structure during the nominal unfolding process.

The W-FPCP model is constructed using two local triangular-panel subsystems. Each local triangular subsystem contains six projected weighting parameters. These weights are first calibrated by minimizing the mismatch between the W-FPCP-predicted vertex trajectories and the bar-and-hinge reference trajectory for the nominal $100^\circ \rightarrow 180^\circ$ unfolding motion. As shown in Fig. 6, the calibrated W-FPCP closely reproduces the vertex trajectories generated by the bar-and-hinge model.

To further examine the robustness of the calibrated weights, we keep the optimized weights fixed and simulate W-FPCP from perturbed initial vertex configurations. The structure rotates to a different orientation and starts with the same initial folding angle, while small vertex-level perturbations are introduced to represent panel expansion and twisting disturbances. The corresponding bar-and-hinge trajectory is generated from the same perturbed initial configuration, and no re-optimization is performed. As shown in Figs. 7 and 8,

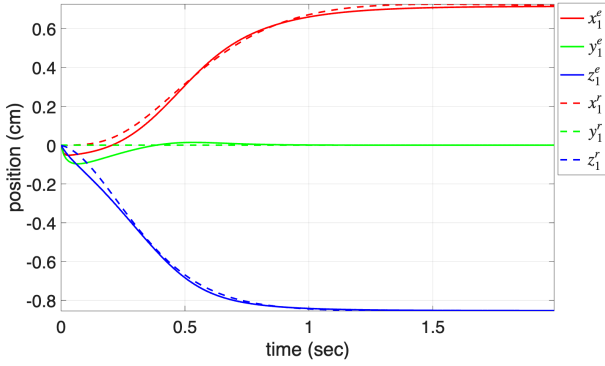


Fig. 6: Comparison of coordinate history of trajectory two between calculated results (solid line) and reference data (dashed line) for Vertex 1 for two panel structure nominal simulation.

the fixed-weight W-FPCP model remains able to reproduce the main trajectory trend under these initial perturbations.

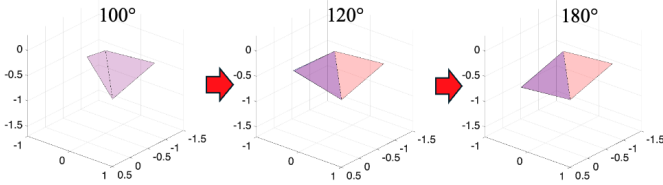


Fig. 7: Reference bar-and-hinge model (red) and calculated (blue) states of the two-panel structure during the unfolding process with different configuration and noise.

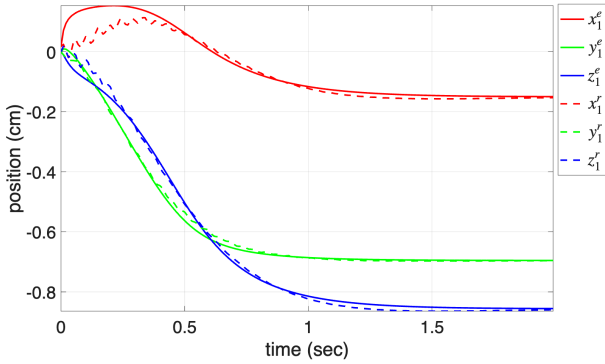


Fig. 8: Comparison of coordinate history of trajectory two between calculated results (solid line) and reference data (dashed line) for Vertex 1 for two panel structure simulation with noise.

B. Kresling Structure

The Kresling pattern is an origami structure that folds unidirectionally and exhibits bistability [32]. When a continuous axial force, accompanied by a rotational torque, is applied along the central symmetric axis of the Kresling origami, it induces a unidirectional collapse or extension of the structure. All vertices move with uniform velocity along this axis at every moment, maintaining a synchronized folding motion.

The Kresling pattern's bistable nature implies two stable equilibrium states, where the structure can maintain its configuration without additional external forces. The strain energy model governs the convergence to one of these equilibrium states, which depends on two key parameters at the initial unstable state: twist angle and height. We use the percentage of folding as a representative metric to simplify the characterization of the initial unstable states. If the initial folding percentage falls below a critical threshold, the structure stabilizes at state 1, corresponding to 0% folded, as shown in Fig. 9(b). In contrast, if the initial folding percentage exceeds this threshold, the structure settles at state 2, corresponding to 100% folded, as shown in Fig. 9(c). For a given Kresling origami design, this threshold can be determined on the basis of its geometric and material properties.

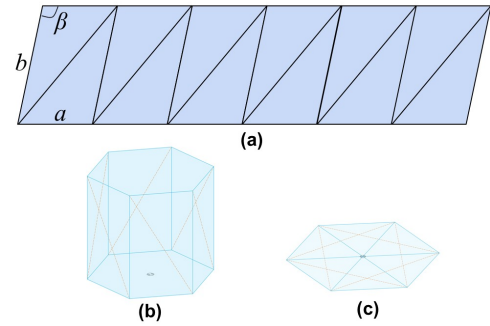


Fig. 9: An example of (a) Kresling pattern with parameters in their graph representations, (b) Equilibrium state 1 (0% folded), and (c) Equilibrium state 2 (100% folded).

The Kresling pattern consists of uniform triangular panels that define the structural geometry. These panels are characterized by three fundamental parameters: The bottom length of the triangular panel is denoted as a , the side length as b , and the number of sides in the polygonal cross-section as n . These parameters define the size and shape of each triangular panel within the structure, as shown in Fig. 9(a). Based on these geometric properties, the desired triangular configuration, $\tilde{\mathbf{r}}_{i,j,k}^{\text{panel}} = [\tilde{\mathbf{r}}_i^{\text{panel}\top}, \tilde{\mathbf{r}}_j^{\text{panel}\top}, \tilde{\mathbf{r}}_k^{\text{panel}\top}]^\top$, of the Kresling pattern can be formulated as

$$\tilde{\mathbf{r}}_i^{\text{panel}} = [0 \quad 0]^\top, \quad (33a)$$

$$\tilde{\mathbf{r}}_j^{\text{panel}} = [a \quad 0]^\top, \quad (33b)$$

$$\tilde{\mathbf{r}}_k^{\text{panel}} = [-b \cos \beta \quad b \sin \beta]^\top, \quad (33c)$$

where β is defined as

$$\beta = \frac{\pi}{n} + \arcsin\left(\frac{b}{a} \sin\left(\frac{\pi}{n}\right)\right). \quad (34)$$

The hinge configuration in the Kresling pattern defines the relative angles between two adjacent panels during transitions between the folded and unfolded states, that allows panel deformations while maintaining the structural integrity of the origami pattern. In the simulation, the system target state is set in a fully folded and unfolded configuration, i.e., the equilibrium state 1 in Fig. 9(b), where the target configurations for hinge consensus are determined. There are two distinct

hinge configurations in the Kresling pattern, each associated with the corresponding target formation, $\tilde{\mathbf{r}}_{i,k,l}^{\text{hinge1}}$ and $\tilde{\mathbf{r}}_{i,j,l}^{\text{hinge2}}$, defined in (14). For the configuration with $\phi = 0$, $\mathbf{q}_{\iota,\kappa}$, $\iota, \kappa = i, j, k, l, \iota \neq \kappa$ are defined by

$$\mathbf{q}_{k,l} = \mathbf{q}_{i,j} = [-b \cos \beta \quad -b \sin \beta \quad 0]^\top, \quad (35a)$$

$$\mathbf{q}_{\iota,j} = [-a \quad 0 \quad 0]^\top, \quad (35b)$$

$$\mathbf{q}_{k,j} = [-a - b \cos \beta \quad -b \sin \beta \quad 0]^\top. \quad (35c)$$

Similarly, for the configuration with $\phi = \pi - \frac{(n-2)\pi}{n}$, $\mathbf{q}_{\iota,\kappa}$, $\iota, \kappa = i, j, k, l, \iota \neq \kappa$ are defined by

$$\mathbf{q}_{k,l} = \mathbf{q}_{i,j} = [a \quad 0 \quad 0]^\top, \quad (36a)$$

$$\mathbf{q}_{\iota,j} = [-a - b \cos \beta \quad -b \sin \beta \quad 0]^\top, \quad (36b)$$

$$\mathbf{q}_{k,j} = [-b \cos \beta \quad -b \sin \beta \quad 0]^\top. \quad (36c)$$

The geometric dimensions of the Kresling pattern are set as $a = 5$, $b = 8.66$, and $n = 6$.

To incorporate weighting parameters into the proposed FPCP, the parameter optimization problem formulated in (32) is numerically solved to obtain optimal weights associated with each Laplacian matrix. For demonstration purposes, the observed reference data utilized in this simulation is generated from a geometric kinematic model, assuming the origami structure folds at a constant angular rotation speed [33]. To effectively capture and reflect diverse dynamic behaviors and enhance robustness, randomized time intervals, Δt_κ , are selected throughout the simulation. In this simulation example, time variable t here denotes a continuous-time evolution parameter associated with the consensus dynamics. Although it is not explicitly identified with physical actuation time, it serves as a time-like variable that parameterizes the progression of the system during the reconfiguration process.

The optimized weights are integrated into the dynamic model, and the resulting simulated vertex trajectories are compared directly against the two reference trajectories from the geometric model with one set of weights. The simulated vertex coordinate histories using the optimized parameters and their corresponding reference trajectories are illustrated in Figs. 10 and 11. Trajectory 1 in Fig. 10 starts from an initially unstable, 25%-folded configuration toward the equilibrium (0%-folded), while trajectory 2 in Fig. 11 starts from 75%-folded configuration toward another equilibrium (100%-folded) state. As clearly depicted in these plots, the vertex positions predicted by the optimized dynamic model exhibit a close agreement with the reference data. The trajectories generated using optimized weights closely reproduce the reference coordinate histories and terminal configurations for the selected geometric reconfiguration cases.

To quantitatively assess the accuracy of the parameter identification procedure, the mean squared errors (MSE) between the simulated vertex positions (obtained with optimized parameters) and the reference trajectories (obtained from the geometric model) are computed. These error metrics are summarized in Table II.

Using the optimized parameters determined by the W-FPCP, Fig. 12 illustrates the dynamic unfolding/folding process of

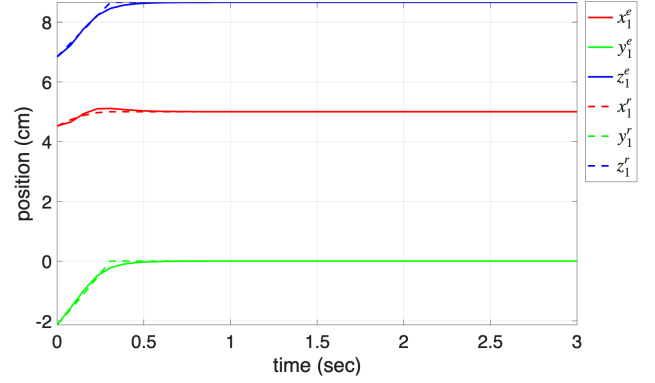


Fig. 10: Comparison of coordinate history of trajectory 1 between calculated results (solid line) and reference data (dashed line) for Vertex 1.

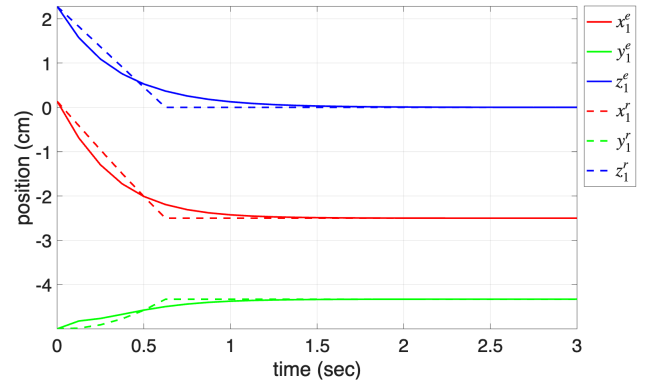


Fig. 11: Comparison of coordinate history of trajectory 2 between calculated results (solid line) and reference data (dashed line) for Vertex 1.

the Kresling origami pattern, respectively. Simulation results demonstrate that, under the W-FPCP with optimized weights, the origami structure naturally evolves toward the stable state 1 (fully unfolded) or stable state 2 (fully folded). The simulated states closely match the reference states derived from the geometric kinematic model, indicating that the proposed model accurately reproduces the observed reconfiguration trajectory. The congruence between simulation results from the W-FPCP and the reference data supports the effectiveness of the proposed weighted consensus modeling framework for representing origami reconfiguration behavior.

The single optimized weight set in this example is interpreted as a compact effective parameterization for the selected Kresling reconfiguration trajectories, rather than a globally valid parameter set for all folding percentages. Because the Kresling dynamics are nonlinear and branch-dependent, fitting the weights over the entire range of folding percentages can reduce trajectory-specific accuracy, while fitting only a short segment may degrade prediction outside that segment. This reflects an expressiveness limitation of using one constant set of W-FPCP weights. Developing piecewise multi-set weighting strategies for different folding regimes is left for future work.

	Non-weighted FPCP	W-FPCP with optimized weights
MSE	129.4218	0.3276

TABLE II: MSE of non-weighted FPCP and W-FPCP relative to reference trajectory

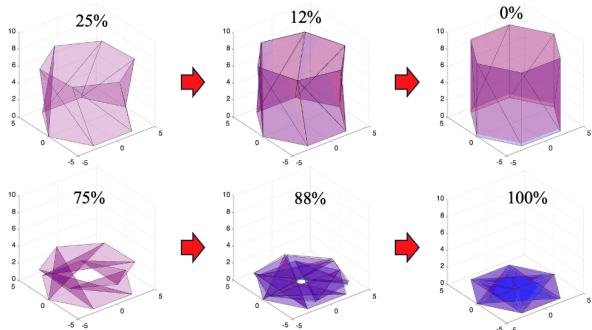


Fig. 12: Reference (red) and calculated (blue) states of the Kresling pattern during the unfolding process of trajectories 1 and 2.

VI. CONCLUDING REMARKS

This paper proposed the frame-projected consensus protocol (FPCP) to model the folding and unfolding dynamics of triangulated origami structures. By projecting each local vertex state onto a local two-dimensional frame of its panel or hinge plane before applying the consensus protocol, FPCP preserves the geometry of every panel throughout reconfiguration. The weighted extension of FPCP, named W-FPCP, is then proposed to better embed the physical attributes of the origami structure and improve the modeling fidelity. Theoretical analysis of the proposed method to establish its stability and convergence properties has also been provided. In addition, a data-fitting parameter estimation framework has been introduced to estimate model weights from observed vertex trajectories. Numerical simulations on a two-panel structure and a Kresling pattern demonstrated that the proposed W-FPCP closely tracks the reference data and naturally converges to an equilibrium condition, even under initial perturbations. These results support the ability of the proposed framework to represent origami reconfiguration trajectories in agreement with the chosen geometric reference model. Future work will extend the proposed framework to enable online parameter adaptation, multi-set of parameter fitting, and validation of the model experimentally on various origami prototypes.

VII. APPENDIX I

PROOF OF THEOREM 4.2

Proof. Define $\delta = \tilde{M}_{\text{panel}} \mathbf{x}_{i,j,k} - \tilde{\mathbf{r}}_{i,j,k}^{\text{panel}}$. Since $\tilde{M}_{\text{panel}} \tilde{M}_{\text{panel}}^{\top} = I_3 \otimes (M_{\text{panel}} M_{\text{panel}}^{\top}) = I_6$, the dynamics in (10) implies

$$\dot{\delta} = \tilde{M}_{\text{panel}} \dot{\mathbf{x}}_{i,j,k} = -L_2 \delta.$$

Thus, the projected error follows the standard formation-consensus dynamics in the local 2D frame. Let $V(\delta) = \frac{1}{2} \|\delta\|^2$, then

$$\dot{V} = \delta^{\top} \dot{\delta} = -\delta^{\top} L_2 \delta \leq 0,$$

where $L_2 = L(K_3) \otimes I_2$ is symmetric positive semidefinite. By LaSalle's invariance principle, $\delta(t)$ converges to the largest invariant set satisfying $L_2 \delta = 0$. Since K_3 is connected,

$$\ker L_2 = \{(\mathbf{1}_3 \otimes I_2) \mathbf{c} : \mathbf{c} \in \mathbb{R}^2\}.$$

Therefore, $\delta(t) \rightarrow (\mathbf{1}_3 \otimes I_2) \mathbf{c}$ for some $\mathbf{c} \in \mathbb{R}^2$, or equivalently,

$$\tilde{M}_{\text{panel}} \mathbf{x}_{i,j,k}(t) \rightarrow \tilde{\mathbf{r}}_{i,j,k}^{\text{panel}} + (\mathbf{1}_3 \otimes I_2) \mathbf{c}.$$

Taking the differences between any two vertices eliminates the translation term and gives

$$M_{\text{panel}}(\mathbf{x}_l(t) - \mathbf{x}_\kappa(t)) \rightarrow \tilde{\mathbf{r}}_l^{\text{panel}} - \tilde{\mathbf{r}}_\kappa^{\text{panel}}, \quad l, \kappa \in \{i, j, k\}.$$

This proves convergence to the desired projected triangular formation, up to a rigid translation in the local 2D frame. \square

VIII. APPENDIX II

PROOF OF COROLLARY 2.1

Proof. The proof follows directly from Theorem IV.2 by replacing the unweighted Laplacian L_2 with the weighted Laplacian $\Omega_{i,j,k}$. Similarly, for $\delta = \tilde{M}_{i,j,k} \mathbf{x}_{i,j,k} - \tilde{\mathbf{r}}_{i,j,k}$, we have $\dot{\delta} = -\Omega_{i,j,k} \delta$, where $\tilde{M}_{i,j,k} \tilde{M}_{i,j,k}^{\top} = I_6$. Since $\Omega_{i,j,k}$ is symmetric positive semidefinite, the W-PFCP for a single panel gives

$$\delta(t) \rightarrow \ker(\Omega_{i,j,k}).$$

Using the null-space condition in (28), there exists $\mathbf{c} \in \mathbb{R}^2$ such that $\delta(t) \rightarrow (\mathbf{1}_3 \otimes I_2) \mathbf{c}$. Similar to Theorem IV.2, we have

$$M_{i,j,k}(\mathbf{x}_l(t) - \mathbf{x}_\kappa(t)) \rightarrow \tilde{\mathbf{r}}_l - \tilde{\mathbf{r}}_\kappa, \quad l, \kappa \in \{i, j, k\}.$$

This completes the proof. \square

IX. APPENDIX III

PROOF OF THEOREM 4.5

Proof. Using the definitions of H_q and \mathbf{g}_q , the dynamics on $[t_q, t_{q+1})$ can be written as

$$\dot{\mathbf{x}} = -H_q \mathbf{x} + \mathbf{g}_q.$$

By the common-equilibrium condition (30), $H_q \mathbf{x}^* = \mathbf{g}_q$ for every q . Defining $\mathbf{e}(t) = \mathbf{x}(t) - \mathbf{x}^*$, we obtain the piecewise-linear error dynamics

$$\dot{\mathbf{e}} = -H_q \mathbf{e}, \quad t \in [t_q, t_{q+1}).$$

From Corollary IV.1.1, $\hat{W}_{\Gamma,q}$, $\Gamma = 1, \dots, m + 2h$, is positive semidefinite. Hence, each H_q is positive semidefinite. Moreover, by definition, $H_q \mathbf{n} = 0$ for every $\mathbf{n} \in \mathcal{N}$ and every q . Since \mathcal{N}^\perp is invariant under H_q , the error component $\mathbf{e}_\perp := P_{\mathcal{N}^\perp} \mathbf{e}$ satisfies $\dot{\mathbf{e}}_\perp = -H_q \mathbf{e}_\perp$. Consider $V(\mathbf{e}_\perp) = \frac{1}{2} \|\mathbf{e}_\perp\|^2$. For $t \in [t_q, t_{q+1})$,

$$\dot{V} = \mathbf{e}_\perp^{\top} \dot{\mathbf{e}}_\perp = -\mathbf{e}_\perp^{\top} H_q \mathbf{e}_\perp.$$

Using (31), we obtain

$$\dot{V} \leq -\mu \|\mathbf{e}_\perp\|^2 = -2\mu V.$$

Therefore, $V(t) \leq e^{-2\mu t} V(0)$. Hence, on each interval,

$$V(t) \leq e^{-2\mu(t-t_q)} V(t_q), \quad t \in [t_q, t_{q+1}).$$

Since $\mathbf{e}_\perp(t)$ is continuous at each switching time t_q , the value of the common Lyapunov function does not jump, i.e., $V(t_q^+) = V(t_q^-)$. Putting the interval inequalities in sequences gives

$$V(t) \leq e^{-2\mu(t-t_0)}V(t_0), \quad t \geq t_0.$$

Consequently,

$$\|\mathbf{e}_\perp(t)\| \leq e^{-\mu(t-t_0)}\|\mathbf{e}_\perp(t_0)\|,$$

which proves exponential convergence of the component orthogonal to \mathcal{N} . \square

REFERENCES

- [1] D. Rus and C. Sung, "Spotlight on origami robots," *Science Robotics*, vol. 3, no. 15, p. eaat0938, 2018.
- [2] M. Johnson, Y. Chen, S. Hovet, S. Xu, B. Wood, H. Ren, J. Tokuda, and Z. T. H. Tse, "Fabricating biomedical origami: a state-of-the-art review," *International Journal of Computer Assisted Radiology and Surgery*, vol. 12, pp. 2023–2032, 2017.
- [3] M. Hwang, G. Kim, S. Kim, and N. S. Jeong, "Origami-inspired radiation pattern and shape reconfigurable dipole array antenna at c-band for cubesat applications," *IEEE Transactions on Antennas and Propagation*, vol. 69, no. 5, pp. 2697–2705, 2020.
- [4] D. Rus and M. T. Tolley, "Design, fabrication and control of origami robots," *Nature Reviews Materials*, vol. 3, no. 6, pp. 101–112, 2018.
- [5] L. Fei and D. Sujan, "Origami theory and its applications: a literature review," in *Proceedings of World Academy of Science, Engineering and Technology*, no. 73. World Academy of Science, Engineering and Technology (WASET), 2013, p. 1131.
- [6] K. Liu and G. H. Paulino, "Nonlinear mechanics of non-rigid origami: An efficient computational approach," *Proceedings of the Royal Society A: Mathematical, Physical and Engineering Sciences*, vol. 473, no. 2206, p. 20170348, Oct 2017.
- [7] E. Filipov, K. Liu, T. Tachi, M. Schenk, and G. Paulino, "Bar and hinge models for scalable analysis of origami," *International Journal of Solids and Structures*, vol. 124, pp. 26–45, 2017.
- [8] S. R. Woodruff and E. T. Filipov, "A bar and hinge model formulation for structural analysis of curved-crease origami," *International Journal of Solids and Structures*, vol. 204-205, pp. 114–127, 2020.
- [9] Y. Hu, Y. Zhou, K.-W. Kwok, and K. Sze, "Simulating flexible origami structures by finite element method," *International Journal of Mechanics and Materials in Design*, vol. 17, 12 2021.
- [10] M. Moshtaghzadeh, E. Izadpanahi, and P. Mardanpour, "Prediction of fatigue life of a flexible foldable origami antenna with Kresling pattern," *Engineering Structures*, vol. 251, p. 113399, 01 2022.
- [11] D. Zhang, "A Data-driven Framework for Mechanics Analysis of Origami Structures Using Machine Learning Methods," 1 2023.
- [12] L. M. Fonseca, G. V. Rodrigues, and M. A. Savi, "An overview of the mechanical description of origami-inspired systems and structures," *International Journal of Mechanical Sciences*, vol. 223, p. 107316, 2022.
- [13] T. Hull, "Unit origami as graph theory," in *Proceedings of the 2nd International Conference on Origami in Education and Therapy*. New York, 1995, pp. 39–47.
- [14] D. Dureisseix, "An example of geometric origami design with benefit of graph enumeration algorithms," *arXiv preprint arXiv:1510.07499*, 2015.
- [15] T. Kanade, "A theory of origami world," *Artificial intelligence*, vol. 13, no. 3, pp. 279–311, 1980.
- [16] N. Turner, B. Goodwine, and M. Sen, "A review of origami applications in mechanical engineering," *Proceedings of the Institution of Mechanical Engineers, Part C: Journal of Mechanical Engineering Science*, vol. 230, no. 14, pp. 2345–2362, 2016.
- [17] Z. Xia, C. Tian, L. Li, and D. Zhang, "The novel synthesis of origami-inspired mechanisms based on graph theory," *Mechanism and Machine Theory*, vol. 192, p. 105547, 2024.
- [18] K. Yamaguchi, H. Yasuda, K. Tsujikawa, T. Kunimine, and J. Yang, "Graph-theoretic estimation of reconfigurability in origami-based metamaterials," *Materials & Design*, vol. 213, p. 110343, 2022.
- [19] M. Mesbahi and M. Egerstedt, *Graph Theoretic Methods in Multiagent Networks*. Princeton University Press, 2010.
- [20] W. Ren and R. W. Beard, *Distributed Consensus in Multi-vehicle Cooperative Control*. Springer, 2008, vol. 27, no. 2.
- [21] Y. Lou, G. Shi, K. H. Johansson, and Y. Hong, "Approximate projected consensus for convex intersection computation: Convergence analysis and critical error angle," *IEEE Transactions on Automatic Control*, vol. 59, no. 7, pp. 1722–1736, 2014.
- [22] X. Chen, M.-A. Belabbas, and T. Başar, "Global stabilization of triangulated formations," *SIAM Journal on Control and Optimization*, vol. 55, no. 1, pp. 172–199, 2017.
- [23] A. Nedic, A. Ozdaglar, and P. A. Parrilo, "Constrained consensus and optimization in multi-agent networks," *IEEE Transactions on Automatic Control*, vol. 55, no. 4, pp. 922–938, 2010.
- [24] N. Azizan-Ruhi, F. Lahouti, A. S. Avestimehr, and B. Hassibi, "Distributed solution of large-scale linear systems via accelerated projection-based consensus," *IEEE Transactions on Signal Processing*, vol. 67, no. 14, pp. 3806–3817, 2019.
- [25] P. Yan, H. Huang, M. Meloni, B. Li, and J. Cai, "Mechanical properties inside origami-inspired structures: an overview," *Applied Mechanics Reviews*, vol. 77, no. 1, 2025.
- [26] S. Li, H. Fang, S. Sadeghi, P. Bhowad, and K.-W. Wang, "Architected origami materials: how folding creates sophisticated mechanical properties," *Advanced materials*, vol. 31, no. 5, p. 1805282, 2019.
- [27] J. Zhang and C. Wang, "Deployment behavior and mechanical property analysis of Kresling origami structure," *Composite Structures*, vol. 341, p. 118234, 2024.
- [28] D. Mukherjee and D. Zelazo, "Robustness of consensus over weighted digraphs," *IEEE Transactions on Network Science and Engineering*, vol. 6, no. 4, pp. 657–670, 2018.
- [29] M.-J. Park, O.-M. Kwon, and A. Seuret, "Weighted consensus protocols design based on network centrality for multi-agent systems with sampled-data," *IEEE Transactions on Automatic Control*, vol. 62, no. 6, pp. 2916–2922, 2016.
- [30] Y. Tanaka, R. Dai, and M. Mesbahi, "Dynamic modeling of origami reconfigurations via triangulated consensus," in *American Control Conference*, 2025.
- [31] R. A. Horn and C. R. Johnson, *Matrix Analysis*, 2nd ed. Cambridge: Cambridge University Press, 2013.
- [32] C. Jianguo, D. Xiaowei, Z. Ya, F. Jian, and T. Yongming, "Bistable behavior of the cylindrical origami structure with Kresling pattern," *Journal of Mechanical Design*, vol. 137, no. 6, p. 061406, 2015.
- [33] L. Lu, X. Dang, F. Feng, P. Lv, and H. Duan, "Conical Kresling origami and its applications to curvature and energy programming," *Proceedings of the Royal Society A*, vol. 478, no. 2257, 2022.